Published in final edited form as:
Sci Signal. ; 5(240): ra64. doi:10.1126/scisignal.2002871.

FAM123A Binds Microtubules and Inhibits the Guanine Nucleotide Exchange Factor ARHGEF2 to Decrease Actomyosin Contractility***

Priscila F. Siesser[1,Ψ], **Marta Motolese**[2,Ψ,•], **Matthew P. Walker**[1], **Dennis Goldfarb**[1,3], **Kelly Gewain**[1], **Feng Yan**[1], **Rima M. Kulikauskas**[4], **Andy J. Chien**[4], **Linda Wordeman**[5], and **Michael B. Major**[1]

[1]Department of Cell and Developmental Biology, Lineberger Comprehensive Cancer Center, University of North Carolina at Chapel Hill School of Medicine, Box#7295, Chapel Hill, NC 27599, USA

[2]Howard Hughes Medical Institute, Department of Pharmacology, and Institute for Stem Cell and Regenerative Medicine, University of Washington School of Medicine, Box 357370, Seattle, WA 98195, USA

[3]Department of Computer Science, University of North Carolina at Chapel Hill, Box#3175, Chapel Hill, NC 27599, USA

[4]University of Washington School of Medicine, Department of Medicine, Division of Dermatology, Box 358056 815 Mercer St, Seattle Washington 98109, USA

[5]Department of Physiology and Biophysics, University of Washington School of Medicine, Box 357370, Seattle, WA 98195, USA

Abstract

The FAM123 gene family comprises three members, *FAM123A*, the tumor suppressor *WTX*(*FAM123B*) and *FAM123C*. WTX is required for normal development and causally contributes to human disease, in part through its regulation of β-catenin-dependent WNT signaling. The roles of FAM123A and FAM123C in signaling, cell behavior and human disease remain less understood. We defined and compared the protein-protein interaction networks for each member of the FAM123 family by affinity purification and mass spectrometry. Protein localization and functional studies suggest that the FAM123 family members have conserved and divergent cellular roles. In contrast to WTX and FAM123C, we found that microtubule-associated proteins were enriched in the FAM123A protein interaction network. FAM123A interacted with and tracked dynamic microtubules in a plus-end direction. Domain interaction experiments

To whom correspondence should be addressed: Michael B. Major, Lineberger Comprehensive Cancer Center, University of North Carolina at Chapel Hill Box#7295, Chapel Hill, NC27599, benmajor@med.unc.edu, Phone: 919-966-9258, Fax: 919-966-8212.
•I.N.M. Neuromed, Pozzilli, Italy (present address).
ΨThese authors contributed equally to this work.

Author contributions: M.B.M, P.S. and M.M designed the experiments and analyzed the data; these and all other authors performed the experiments. M.B.M., F.Y and D.G performed the MS analysis. P.S, M.M and M.B.M wrote the manuscript.

Competing interests: The authors declare that they have no competing interests.

Data availability: The data associated with this manuscript may be downloaded from ProteomeCommons.org Tranche using the following hash: SG+Lb+X7PAOmf9pdlyQREvVmA7sOZX/iwKCV7zQBvmofGaBNxvXg8D9dZkUs5CgbiDMIBp6JlNW1fh0EgeWb8SOaaxMAAAAAAAADcA==

revealed a 'SKIP' amino acid motif in FAM123A that mediated interaction with the microtubule tip tracking proteins EB1 and EB3, and therefore with microtubules. Cells depleted of FAM123A showed compartment-specific effects on microtubule dynamics, increased actomyosin contractility, larger focal adhesions and decreased cell migration. These effects required binding of FAM123A to and inhibition of the guanine nucleotide exchange factor ARHGEF2, a microtubule-associated activator of RhoA. Together, these data suggest that the 'family-unique' SKIP motif enables FAM123A to bind EB proteins, localize to microtubules and coordinate microtubule dynamics and actomyosin contractility.

Introduction

The FAM123 gene family comprises three members: *FAM123A*, which is also known as *AMER2; FAM123B*, which is also known as *WTX, AMER1* and *OSCS*; and *FAM123C*. The founding member, *FAM123B* (hereafter referred to as *WTX*) plays fundamental roles in normal development and human disease. Mutations in *WTX* contribute to various diseases, such as Wilms tumor, a pediatric kidney cancer (1, 2), and osteopathia striata congenita with cranial sclerosis (OSCS), an X-linked developmental disorder that causes bone-related defects in females (3) and is lethal in males, often at embryonic or neonatal developmental stages. Mice lacking *WTX* display various developmental abnormalities in tissues of mesenchymal origin, such as increased bone mass and decreased adipose tissue (4). Cellular and molecular analyses of these tissues indicate a critical role for WTX in regulating cell differentiation programs in mesenchymal progenitors.

Mass spectrometry-based proteomic dissection of WTX protein complexes has revealed several core components of the β-catenin-dependent WNT signal transduction pathway, including β-catenin (encoded by *CTNNB1*), βTrCP2 (encoded by *FBXW11*) and adenomatous polyposis coli (APC) (5, 6). Subsequent functional studies in various cells and organisms demonstrated that WTX inhibits WNT pathway activity (4, 5, 7). *In vitro* studies and cell-based assays suggest that WTX promotes β-catenin ubiquitination and subsequent proteasomal degradation, perhaps by serving as a membrane-bound scaffold for the β-catenin phosphorylation complex (5-8).

Of the FAM123 family members, WTX and FAM123A share greatest homology, particularly in their N-termini (6, 9, 10). Two conserved functional domains in WTX and FAM123A have been identified and characterized (6, 11). First, both proteins share an N-terminal phosphatidylinositol(4,5)-bisphosphate-binding domain that localizes these proteins to the plasma membrane and is required for WTX- and FAM123A-mediated inhibition of WNT signal transduction. Second, WTX and FAM123A directly bind to APC and regulate its subcellular distribution, recruiting it from the microtubule tip complex to the plasma membrane. Although the functional consequences of this redistribution are not completely understood, the role for APC in microtubule stabilization and maintenance of cell-cell junctions suggests that WTX and FAM123A may influence directional cell migration and polarity (6). Whether the more distantly related family member FAM123C also regulates WNT signaling, localizes to the plasma membrane or binds APC remains unknown.

In contrast to WTX, the cellular, developmental and disease contributions of FAM123A and FAM123C remain less understood. Thus, we defined and compared the protein-protein interaction networks for each member in the FAM123 family. Functional annotation of the resulting protein interaction network and comparative protein dynamic studies supports both conserved and divergent functions for the FAM123 family members. Here we report a 'family-unique' function for FAM123A in controlling communication between the microtubule and actomyosin cytoskeletal networks. We found that FAM123A binds the microtubule plus-end tracking proteins EB1 and EB3, moves on microtubules, controls

microtubule dynamics, actomyosin organization and cell migration. We present a model wherein FAM123A binds to and inhibits GEF-H1 (encoded by *ARHGEF2*) to decrease actomyosin contractility.

Results

Comparative proteomics of the WTX family reveals shared and unique interactions

To provide insight into the cellular functions of FAM123A and FAM123C, we defined their protein interaction networks by shot-gun liquid chromatography–tandem-mass spectrometry of affinity purified protein complexes. Integration of the resulting protein interaction networks with a previously defined WTX protein interaction network revealed shared and unique protein-protein interactions (Fig. 1A and Table S1). Consistent with the homology relationships within the family, FAM123A and WTX shared several common interacting proteins; in contrast, the FAM123C protein interaction network was distinct (Fig. 1B and Table S1).

Because of their homology, overlapping protein interaction networks and shared function as inhibitors of WNT signaling, protein interactions from the WTX and FAM123A networks were validated. FAM123A or WTX protein complexes were isolated by streptavidin affinity purification from HEK293T cells and associated endogenous proteins were detected by Western blot. Whereas both WTX and FAM123A proteins associated with APC and βTrCP1 (encoded by *BTRC*) and βTrCP2 (encoded by *FBXW11*), WTX specifically bound β-catenin, confirming the proteomic data (Fig. 1C). These results strengthen models in which WTX and FAM123A functionally regulate β-catenin-dependent WNT signaling at the level of the destruction complex, most likely through interactions with APC, βTrCP1 or βTrCP2.

We chose to further investigate the enrichment of microtubule associated proteins in the FAM123A protein interaction network (Fig. 1A, green nodes), such as EB1 (encoded by *MAPRE1*), an obligate component of the microtubule plus-end tip tracking protein complex (12-14). Western blot analysis of affinity purified protein complexes revealed an interaction between FAM123A and endogenous EB1, but not between WTX and EB1 (Fig. 1C). Additionally, several other proteins in the FAM123A network bind to the microtubule cytoskeleton: the microtubule affinity regulating kinases MARK2 and MARK3, GEF-H1, EB3 (encoded by *MAPRE3*), ACF7 (encoded by *MACF1*), CLASP2 and APC (15-20) (Table S1). By affinity purification and mass spectrometry, these proteins are frequently observed FAM123A interacting proteins, and are largely absent from the WTX protein interaction network (Fig. 1A).

FAM123A moves on growing microtubules

WTX and FAM123A, but not FAM123C, localize predominantly to the cytoplasmic face of the plasma membrane through interactions with phospholipids (Fig. S1) (6). Given the relative enrichment of microtubule-associated proteins in the FAM123A protein interaction network, we hypothesized that a pool of FAM123A might localize to and move on microtubules. Imaging of Venus-FAM123A or Venus-WTX in live HT1080 human sarcoma cells (Fig. 1D) indicated that both proteins exhibited mainly membranous distribution, seemed to be enriched at cell ruffles and induced cell death when overexpressed. In cells expressing low to moderate amounts FAM123A (movie S1), but not WTX (movie S2), localized to filamentous structures resembling microtubules. This localization pattern was often polarized with respect to the direction of cell movement; of 142 cells with low to moderate expression of FAM123A, 94 cells showed FAM123A decorating filamentous structures polarized in the direction of cell movement. Co-localization of FAM123A and α-

tubulin confirmed the microtubule localization suggested by live cell imaging (Fig. 1E), which was abolished by the addition of the microtubule destabilizing drug nocodazole. By high resolution live cell imaging, EGFP-FAM123A predominantly moves on segments of microtubules and was also observed as dots that moved on linear trajectories from the cell body toward the cell periphery (movie S3). Thus, both comparative proteomics and live cell imaging demonstrate that FAM123A and not WTX associates with and moves on microtubules.

FAM123A interacts with APC and EB1 through distinct domains

Mass spectrometry and Western blot analysis revealed that FAM123A associated with the plus-end tracking protein EB1 (Fig. 1A and Fig. 1C). Stably expressed HA-tagged FAM123A was detected in protein complexes isolated by immunopurification of endogenous EB1 (Fig. 2A). To demonstrate the interaction between the endogenous proteins, we generated an antibody against FAM123A and confirmed its specificity with two non-overlapping *FAM123A*-specific siRNAs (Fig. 2B and C). In both HEK293T and HeLa cells, endogenous FAM123A was detected within endogenous EB1 immunopurified protein complexes (Fig. 2D and E). Confocal Z-series images of HeLa cells expressing EGFP-FAM123A and immunofluorescently labeled for endogenous EB1 demonstrated basal co-localization of these proteins with increased intensity at the microtubule distal ends towards the leading edge (Fig. 2F).

APC directly interacts with EB1 and FAM123A. To determine whether FAM123A indirectly binds EB1 through APC (21), we purified FAM123A from cells transfected with siRNAs targeting either *APC* or *EB1* and found that FAM123A interacts with EB1 in the absence of APC, and similarly interacts with APC after silencing of EB1 (Fig. 3A). These results suggest that FAM123A independently binds APC and EB1. Although WTX associates with APC, it did not affinity purify with EB1 (Fig. 1C). To map the domains of FAM123A that interacted with APC and EB1, we generated a series of FAM123A deletion mutants based on homology within the WTX family and on secondary structure prediction for FAM123A (http://robetta.bakerlab.org/). Affinity purification of full length FAM123A protein or the truncated fragments from cells expressing EB1 or APC indicated that FAM123A interacted with EB1 through its extreme C-terminus, specifically amino acids 457-552 (Fig. 3B) and with APC through an N-terminal domain comprising amino acids 261-349 (Fig. 3C). Additionally, FAM123A interacted with βTrCP2 through a C-terminal region encompassing residues 261-470, which overlaps with the APC binding domain (Fig. 3D and S2). These results demonstrate that FAM123A independently interacts with EB1 and APC through non-overlapping domains.

FAM123A interacts with EB proteins through the EB binding motif “Ser-x-Ile-Pro”

Many plus-end tracking proteins contain a characteristic EB-binding motif, which is defined by a Ser-x-Ile-Pro (SxIP) consensus (Fig. 4A) (22), and which enables direct binding to EB1 and EB3 and consequently localization to the growing microtubule plus-end. We found a SKIP$^{487\text{-}490}$ and a TKIP$^{518\text{-}521}$ motif within FAM123A, both of which are in the EB1 binding region identified by domain-mapping (Fig. 3B). To determine if the SKIP$^{487\text{-}490}$ motif is required for binding to EB1 and EB3 we created a mutant in which Ile^{489} and Pro^{490} residues were changed to alanine (FAM123A-IPAA) (Fig. 4A). Affinity purification and Western blot analysis revealed that in contrast to wild-type FAM123A, the IPAA mutant did not pull-down EB1 or EB3 (Fig. 4B and 4C). These results demonstrate that the SKIP$^{487\text{-}490}$ motif in FAM123A is necessary for association with EB1 and EB3; whether the TKIP$^{518\text{-}521}$ motif contributes to binding in the presence of the SKIP$^{487\text{-}490}$ motif remains to be tested.

Many plus-end tracking proteins containing the "SxIP motif" bind a coiled coil domain within the C-terminus of EBs, referred to as the EBH domain (17, 22). To determine if FAM123A also binds to the EBH domain of EB1, we generated two EB1 deletion constructs that encoded the N-terminal microtubule binding domain (AA 1-135) or the C-terminal EBH domain (AA 136-268). Affinity purification of FAM123A from cells co-expressing these EB1 truncations revealed an association between FAM123A and the EBH domain of EB1 (Fig. 4D). Thus, FAM123A interacts with the C-terminal region of EB1 through the consensus EB1 binding motif "SxIP".

The SxIP motif targets functionally and structurally unrelated plus-end tracking proteins to growing microtubule ends in an EB dependent manner (22). To determine if FAM123A microtubule localization and plus-end tracking require EB association, we compared the protein distribution and dynamics of FAM123A and FAM123A-IPAA by live cell imaging (Fig. 4E and movie S4 and movie S5). Wild-type FAM123A coated the distal ends of the microtubule and co-tracked with EB3 in the cell body (movie S4). In contrast, FAM123A-IPAA exhibited decreased EB3-associated plus-end tip tracking and microtubule decoration, coating very few microtubule stretches at the cell periphery (movie S5). A C-terminal fragment of FAM123A which contains the $SKIP^{487-490}$ EB-interaction motif did not decorate the microtubule lattice, but rather behaved as a classic plus-end microtubule binding protein showing robust EB3-associated tip tracking (Fig. S3 and movie S6). Mutation of the $SKIP^{487-490}$ motif completely abolished microtubule co-localization and EB3-associated tip tracking (Fig. S3 and movie S7).

Despite the autonomous microtubule binding capability of EB proteins *in vitro*, FAM123A could influence EB1 loading or distribution on microtubules *ex vivo*. However, depletion of FAM123A in HeLa cells did not affect the subcellular distribution of endogenous EB1 (Fig. 4F). To complement the loss-of-function approach, we localized EB1 in cells stably over-expressing FAM123A (Fig. S4). Forced expression of FAM123A, but not FAM123A-IPAA, re-localized EB1 to the microtubule lattice at the bottom of the cell and to the plasma membrane more apically. Although consistent with its ability to bind EB1, it remains to be seen whether its re-distribution following FAM123A over-expression occurs normally. Together these data demonstrate that: (i) FAM123A is a microtubule associated protein with EB-dependent plus-end tip tracking capabilities, (ii) FAM123A binds EB proteins through the $SKIP^{487-490}$ motif, (iii) FAM123A predominantly decorates the microtubule lattice at the cell periphery in a largely EB-dependent fashion, and (iv) FAM123A silencing does not affect EB1 subcellular localization.

EB-protein association is not required for FAM123A regulation of Wnt signaling

Of the three FAM123 family members, only FAM123A contains a SxIP motif, which is consistent with the lack of association between WTX and EB1 (Fig. 1A and 1C). Given this unique protein interaction within the FAM123 family, we predicted that the EB1 association would be dispensable for the common functions of WTX and FAM123A, such as regulation of β-catenin dependent WNT signaling (5, 7, 11). Indeed, siRNA-based knockdown of FAM123A or WTX increased the activity of a β-catenin reporter gene (Fig. S5A). In a gain-of-function approach, over-expression of FAM123A or FAM123A-IPAA reduced WNT3A-dependent reporter activation in a concentration dependent manner (Fig. S5B and C). These data suggest that the ability of FAM123A to modulate the Wnt/β-catenin pathway is independent of its interaction with EB1 and microtubules.

FAM123A controls microtubule organization and growth rates

Because FAM123A bound EB proteins and moved on microtubules, we tested whether its loss affected microtubule organization and dynamics. siRNA-mediated silencing of

FAM123A in HeLa cells induced disorganization of the microtubule network with excessively curved microtubules and increased microtubule density (Fig. 5A and B). In contrast, siRNA mediated silencing of WTX yielded a distinct microtubule organization (Fig. 5A). We used total internal reflective fluorescence (TIRF) microscopy to image GFP-tagged EB3 in siRNA-transfected HeLa cells and found that FAM123A promotes microtubule growth within the cell body, because cells lacking FAM123A had significantly slower microtubule polymerization (Fig. 5C and D). In contrast, in the absence of FAM123A microtubules demonstrated less dynamic movement near F-actin bundles, particularly near adhesion complexes (Fig. 5D). Thus, FAM123A regulates microtubule dynamics and the overall organization of the microtubule network.

FAM123A inhibits actin contractility by suppressing the GEF-H1-RhoA-ROCK-MLC pathway

In addition to the altered microtubule organization, we noticed that FAM123A-depleted cells had phase dark cortical membranes (Fig. 6A). These observations and the increase in cortical F-actin detected by TIRF microscopy (Fig. 5D) suggested involvement of the signaling pathway that mediates crosstalk between the microtubule and actomyosin cytoskeletal networks (15, 23). Specifically, microtubule depolymerization induces actin stress fiber formation and cell contractility through activation of the Rho-specific exchange factor GEF-H1, which subsequently activates RhoA, Rho kinase (ROCK) and myosin light chain (MLC) (Fig. 6B)(24, 25). In *FAM123A*-silenced HeLa cells, thick and short actin stress fibers were disposed in a non-parallel arrangement and microtubule depolymerization induced by nocodazole treatment resulted in several morphological changes, including thick bundles of contracted actin stress fibers frequently localized at the cell center, kidney-shaped nuclei shifted to the cell periphery, and cytoplasmic pools of free tubulin confined to a small area close to the nucleus or near the cell center (or both) (Fig. 6D). Thus, FAM123A-depleted cells display an altered microtubule network and increased actomyosin contractility that is exacerbated with nocodazole treatment.

We employed multiple experimental approaches to determine whether FAM123A induced actomyosin contractility requires the GEF-H1-RhoA-ROCK-MLC2 pathway. First, treatment of cells with the ROCK inhibitor Y-27632 (26) abolished actin stress fiber formation and cell contractility induced by FAM123A knockdown (Fig. 6C). Second, siRNAs targeting GEF-H1 reversed the actomyosin contractility induced by FAM123A depletion, but did not rescue the disordered microtubule phenotype induced by *FAM123A* silencing (Fig. 6D). By blinded quantitation, 78% of FAM123A depleted cells were scored as displaying increased actomyosin contractility; in the absence of GEF-H1, this was reduced to 38% of cells (Fig. 6E). As was previously reported, silencing of *GEF-H1* resulted in decreased actin bundling (Fig. S6)(24). Third, activation of RhoA was higher in cells depleted of FAM123A than in control siRNA-transfected cells, an effect that required GEF-H1 (Fig. 6F). Fourth, phosphorylation of myosin was increased in *FAM123A* silenced cells, but not in cells in which both FAM123A and GEF-H1 were depleted (Fig. 6G-I). By immunofluorescence, phosphorylated MLC localized primarily to stress fibers near the cell periphery following FAM123A loss (Fig. 6I), compared to the more uniform distribution seen in control siRNA transfected cells. Finally, we employed a serum response factor (SRF) transcriptional activity assay as an indirect readout for RhoA activity and actomyosin contractility (27). *FAM123A*-silencing induced SRF reporter activity in a GEF-H1-dependent fashion (Fig. 6J). FAM123A overexpression repressed SRF-mediated transcription induced by both nocodazole and GEF-H1 over-expression (Fig. 6K). Together, these data demonstrate that FAM123A decreases actin contractility by inhibiting the GEF-H1 pathway and that epistatically, FAM123A functions upstream of GEF-H1.

Because cellular morphology and cytoskeletal organization are particularly sensitive to transfection and siRNA-based off target effects, we further validated the specificity of the FAM123A phenotype. HeLa cells expressing one of two siRNAs that targeted the 3′UTR of *FAM123A* (Fig. S7A) showed an exacerbated actomyosin contractility phenotype following nocodazole treatment, similar to the open reading frame-directed FAM123A#1 and #2 siRNAs. This phenotype was rescued by forced expression of a FAM123A-GFP fusion protein (Fig. S7B). Together these data confirm that FAM123A decreases actomyosin contractility.

FAM123A binds to and inhibits GEF-H1 activity

Proteomic analysis of the FAM123A protein complex identified GEF-H1 as a potential interacting protein, suggesting a molecular mechanism by which FAM123A controls actomyosin contractility (Fig. 1A). First, we confirmed the GEF-H1-FAM123A interaction by Western blot analysis of affinity-purified FAM123A protein complexes or immunopurified GEF-H1 protein complexes (Fig. 7A and B). Endogenous GEF-H1 was detected in affinity purified FAM123A protein complexes (Fig. 7A), and FAM123A immunopurified with endogenous GEF-H1 (Fig. 7B). The FAM123A-IPAA mutant, which lacks the ability to bind EB proteins, also associated with GEF-H1 (Fig. 7A and B). Additionally, we detected the endogenous forms of the microtubule associated proteins CLASP2 and MARK2 in FAM123A affinity purified protein complexes, as was suggested by the FAM123A proteomic analyses (Fig. 7A).

As a first test of the functional relationship between FAM132 and GEF-H1, we assessed the activation status of GEF-H1 in FAM123A-depleted cells by purifying active GEF-H1 with a nucleotide-free mutant of RhoA, RhoA-G17A coupled to GST (28). Western blot analysis of RhoA-G17A pull-downs revealed a significant increase in active GEF-H1following FAM123 Adepletion.(Fig. 7C). We attempted to examine the subcellular localization of GEF-H1 after FAM123A over-expression or knockdown; however, we were unable to visualize microtubule-localization of GEF-H1 using various commercially available antibodies and fixation techniques. We reasoned that an effect of FAM123A on GEF-H1 activity could be indirectly assessed by global interrogation of the GEF-H1 protein interaction network. For this approach, we employed SILAC (stable isotope labeling with amino acids in cell culture)-based quantitative proteomics of immunopurified endogenous GEF-H1 protein complexes from parental cells or cells over-expressing FAM123A. Averaging the SILAC ratios from biological replicates identified GEF-H1 protein interactions that were increased by FAM123A expression, such as the association between GEF-H1 and DSTN, an F-actin depolymerizing protein (29, 30), and those that were decreased by FAM123A expression, such as the association between GEF-H1 and SLK, a kinase involved in actin and microtubule organization (31-33). Together, these data demonstrate that FAM123A controls GEF-H1 activity and GEF-H1 protein-protein interactions.

FAM123A regulates cell adhesion and cell migration

Actin stress fibers and focal adhesions are physically and functionally tethered; increases in cellular contractility or application of external mechanical force induces simultaneous growth of focal adhesions and the attached actin stress fibers (34, 35). To determine if actomyosin contractility induced by FAM123A loss impacted focal adhesions, we visualized vinculin as a marker of focal adhesions (Fig. 8A). Consistent with higher contractility, FAM123A depleted cells had larger adhesions than control cells (Fig. 8A). To assess cell adhesion and spreading assay, we performed real time quantitation of electrical impedance during cell spreading, which revealed no effect of FAM123A silencing during the early stages of cell attachment and spreading (Fig. 8B). However, FAM123A depleted cells had

higher impedance values than control cells after the first hour of cell plating, indicating increased adhesion (Fig. 8C), a phenotype that required GEF-H1 (Fig. 8B and C). We also examined the formation of adhesion complexes by immunostaining during cell spreading (Fig. 8D and S8). Consistent with the results from the cell spreading assay, FAM123A depleted and control cells showed phenotypically similar formation of adhesion and actin stress fibers in the early stages of cell spreading. However, after the first hour, the adhesions in FAM123A depleted cells were larger and had thicker actin stress fibers, effects that were GEF-H1 dependent because cells depleted of both FAM123A and GEF-H1 or GEF-H1 alone resembled the control siRNA transfected cells. Given these cytoskeletal and adhesion phenotypes, we tested whether FAM123A silencing impacted cell migration. HeLa cells transfected with either control or FAM123A siRNAs were plated to confluency, scratched and imaged by live cell microscopy. Compared to control siRNA transfected cells, FAM123A depletion resulted in a 20% decrease in cell migration, which may result from increased adhesion (Fig. 8E).

Discussion

We performed unbiased protein-protein interaction screens to discover new functions for members of the FAM123 protein family. Here, we have characterized a ‘family-unique’ physical and functional relationship between FAM123A and the microtubule and actomyosin cytoskeletal networks. We found that FAM123A binds EB proteins and interacts with dynamic microtubules through its SKIP$^{487\text{-}490}$ motif. FAM123A knockdown resulted in compartment-specific effects on microtubule dynamics, a globally disorganized microtubule network, increased GEF-H1 activity, increased actomyosin contractility, and increased cell adhesion and decreased cell migration.

Members of the FAM123 gene family control β-catenin dependent WNT signaling

FAM123A inhibits β-catenin-dependent WNT signaling (11). Our data both confirm these findings and provide additional mechanistic insight. First, comparative protein-protein interaction studies of WTX and FAM123A revealed a robust association between β-catenin and WTX, but not with FAM123A. Although a low affinity or transient interaction between FAM123A and β-catenin may occur, we interpret our data to suggest that association with β-catenin is not required for regulation of WNT signaling by WTX (or FAM123A). Consistent with this notion, the REA repeats in WTX that are responsible for mediating direct interaction with β-catenin are found only in mammalian orthologues of WTX, although WTX inhibits WNT signaling in Zebrafish and *Xenopus*(7). Based on our findings, it is likely that WTX and FAM123A inhibit WNT signaling through interactions with APC or βTrCP1/2 (or both), which associate with both WTX and FAM123A.

Our data demonstrate that the FAM123A-EB interaction is dispensable for WNT regulation, at least with respect to non-polarized cells grown in two dimensions. In contrast to WTX which is uniformly distributed across human tissues, FAM123A is largely restricted to neuronal tissues(9). These disparities in distribution may provide an explanation as to why the ability to control cytoskeletal dynamics is specific to FAM123A, which may have evolved to remodel the cytoskeleton during neuronal migration(11). Because the FAM123C protein interaction network did not share common protein associations with FAM123A or WTX, our data suggest that FAM123C lacks regulatory functions over WNT signaling, although this remains to be formally demonstrated.

FAM123A tracks growing microtubules

Plus-end tracking proteins comprise a structurally and functionally diverse group of microtubule-associated proteins that accumulate at the ends of growing microtubules (15,

17, 19, 36). Many plus-end tracking proteins have a conserved SxIP motif that directly associates with EB proteins and thus mediates localization to the microtubule plus-end (22). In at least two ways, however, our protein dynamic studies also differentiate FAM123A from other plus-end tracking proteins.

First, unlike EB1 and many plus-end tracking proteins which localize to microtubule tips throughout the cell body, FAM123A predominantly decorates the distal ends of microtubules oriented in the direction of cell movement, a polarized distribution also seen for CLASPs, APC, and CDK5RAP2 (37-40). Through asymmetric distribution to the leading edge, these plus-end tracking proteins modulate microtubule dynamics and consequently promote cell polarization and directional migration (41, 42). We found that FAM123A loss differentially affects microtubule dynamics in different subcellular compartments (Fig. 5). Therefore, it is possible that FAM123A functions to regulate spatially-confined microtubule stability, which presumably contributes to the establishment, maintenance, or modulation of asymmetric cell behavior.

Second, although they bind EB proteins for plus-end tracking, many plus-end tracking proteins can also directly associate with microtubules. By contrast, FAM123A microtubule tracking and localization was largely attenuated in the absence of EB-association; one possibility is that the remaining microtubule localization is due to bridging proteins that tether the N-terminus of FAM123A to the microtubule, such as APC. Moreover, the subcellular distribution of full length FAM123A and the C-terminal fragment are substantially different, although both bind EB proteins and track with assembling microtubule ends. Whereas the C-terminus co-localizes with EB-comets, full-length FAM123A exhibits slower microtubule tracking near the cortex, frequently coating the microtubule lattice. These data suggest that FAM123A may be involved in coupling assembling microtubules to membrane signaling pathways.

FAM123A regulates microtubule dynamics and organization

Like many other EB-dependent plus-end tracking proteins, we found that FAM123A depletion results in a disorganized microtubule network. Whereas FAM123A asymmetrically localized to microtubules in the direction of cell movement, its depletion affected microtubule architecture throughout the entire cell body. FAM123A depletion resulted in decreased microtubule polymerization rates within the cell body and less dynamic and stabilized microtubules in apposition to actin adhesion complexes. Although untested, it is possible that the decreased microtubule polymerization rates occur secondarily to the increased cortical stability because of reprogramming overall tubulin homeostasis. For example, decreases in free tubulin dimers as a result of increased stability in some microtubules may result in global effects on microtubule dynamics (43). It also remains possible that actomyosin contractility induced by FAM123A silencing functions in a feed-forward loop to globally influence microtubule dynamics (44). Although our data do not provide an exact mechanism, we propose that FAM123A may control microtubule dynamics by regulating cortical capture through the tethering of microtubules to the plasma membrane. That is, FAM123A complexes with several plus-end tracking proteins thought to stabilize microtubules at the leading edge, such as EB1, EB3, CLASPs, APC and ACF7 (15). It is possible that in association with these plus-end tracking proteins, FAM123A asymmetrically tracks microtubules in the direction of cell movement and promotes both cortical microtubule stabilization and polarized cargo delivery to the cortical membrane. Because WTX and FAM123A bind phospholipids and localize predominantly to the cytoplasmic membrane, an elaboration on this model might have FAM123A ‘jumping’ off of microtubules onto a phospholipid landing pad, perhaps delivering its associated proteins, such as GEF-H1 and APC, to the leading edge. In agreement with this model, FAM123A

recruits APC to the plasma membrane and drives EB1 to the membrane when over-expressed (Fig. S4)(6, 11).

FAM123A inhibits actomyosin contractility, thereby regulating adhesion and cell migration

Our data suggest that FAM123A binds to and inhibits GEF-H1, a guanine nucleotide exchange factor that localizes to microtubules, is activated by microtubule de-polymerization and activates RhoA-dependent actomyosin contraction (24, 25). We show that FAM123A depletion results in GEF-H1-dependent increased actomyosin contractility, enlarged focal adhesions, increased cellular adhesion and decreased cell migration (Fig. 8). These observations demonstrate that FAM123A is similar to PAK1, PAK4, calpain-6, MARK2 and ERK, all of which regulate GEF-H1 to control spatiotemporal regulation of the actin cytoskeleton (45-54). That said, several important questions remain regarding the precise molecular mechanism by which FAM123A regulates GEF-H1.

First, our data demonstrate that FAM123A is epistatically upstream of GEF-H1 with respect to RhoA, ROCK, MLC2, actomyosin contractility and cell adhesion, but not to microtubule organization (Fig. 6). Therefore, actomyosin contractility likely underlies the FAM123A-dependent cell adhesion phenotype, rather than altered microtubule dynamics. Given the limitations of interpreting cause and effect from siRNA-based experiments, additional studies are needed to more precisely define the role of FAM123A in microtubule dynamics and to understand how that effect is communicated through GEF-H1 to the actomyosin network. Second, as mentioned, the precise mechanism by which FAM123A inhibits GEF-H1 remains to be established. Although we show that ectopic FAM123A binds endogenous GEF-H1 (and vice-versa), it remains to be determined if the endogenous proteins associate. Moreover, we were unable to demonstrate GEF-H1 subcellular co-localization with FAM123A. Third, we found that FAM123A inhibits GEF-H1 in the presence and absence of microtubules. Specifically, the IPAA mutant form of FAM123A which does not bind microtubules associates with GEF-H1 and FAM123A knockdown exacerbates actin contraction in the absence of microtubules (Fig. 8 and Fig, 6, respectively). These data suggest that FAM123A functionally impacts GEF-H1 independently of microtubule polymerization status, similar to TNFα-mediated GEF-H1 activation in tubular epithelia (48, 49). Finally, we found that FAM123A altered the GEF-H1 protein interaction network, which we interpret as further corroborative evidence that FAM123A controls GEF-H1 activity or subcellular localization. The biological implications of these GEF-H1 interactions and their control by FAM123A await further study.

In summary, we found using comparative proteomic analyses of the FAM123 family that FAM123A associates with numerous microtubule-binding proteins. Subsequent protein dynamic studies and functional interrogation revealed that FAM123A controls microtubule polymerization rates, actomyosin contractility and consequently cell adhesion and cell migration.

Materials and Methods

Constructs

FAM123A isoform 2 cDNA was obtained by PCR amplification from clone BCO32653 (OPEN Biosystems). The mutant *FAM123A-IPAA* (Ile^{489}-Pro^{490} mutagenized to Ala^{489}-Ala^{490}) was created by standard PCR-based mutagenesis. The WTX constructs were previously described (5). The EB3-pEGFPN1 and EB3-RFP constructs were provided by A. Akhmanova, Erasmus Medical Center, Rotterdam, Netherlands. The EB1-pEGFPN1 construct was provided by L. Cassimeris, Lehigh University, Bethelehm, PA. EB1-pEGFPN2 and the deletions were obtained amplifying EB1 by PCR from pEGFPN1-EB1

construct. The mCherry-tubulin plasmid was made by replacing GFP at the BsrGI and BamHI sites in pEGFP-Tub with mCherry. The β-catenin–activated Firefly reporter (pBAR) and pcDNA3.1-Flag-APC (AA1-1060) were previously described (5). The SRF-RE reporter was obtained from Promega (pGL4.34[*luc2P*/SRF-RE/Hygro]; Madison, WI). GFP-GEF-H1 was kindly provided by Rafael Garcia-Mata, UNC-Chapel Hill.

Reagents

Wnt3A and control conditioned medium was produced in mouse L cells according to the ATCC protocol. Nocodazole and Y-27632 were purchased from Sigma (M1404 and Y0503, Sigma-Aldrich Corporation, St. Louis, MO).

Tissue culture, transfections and reporter assays

All cells were grown in DMEM supplemented with 10% FBS and 1% penicillin/streptomycin, in a 37 °C humidified incubator with 5% CO_2. Transient transfections of siRNAs were performed with Lipofectamine RNAiMAX, as directed by the manufacturer (Invitrogen Carlsbad, CA). All siRNAs were used at a final concentration of 20 nM and for 72 hours unless otherwise stated. siRNAs targeting human forms of WTX (siRNA#1 and #2), APC, axin1/2 and β-catenin have been previously published (5). The following siRNAs were employed: Control: Stealth M2 from Invitrogen; EB1, AAG UGA AAU UCC AAG CUA AGC (42); FAM123A siRNA#1, GCC GGC UCU GUC UAA AAA G[dT][dT]; FAM123A siRNA#2, GAG AUA UUA UUG CAG ACC AAG AGG; FAM123A siRNA#3, CCU ACG UUC AGU UGU UAG AUA UGC A, FAM123A siRNA#4, CCU CUC AAG AUA AGU CCC UGA GAA U; GEF-H1 siRNA#1, AGC AGG CCA CGG AAC UGG CAU UAC U; GEF-H1 siRNA#2, UCC AUA CAC GCU UCC UCA GCC AGC U; WTX siRNA#3, AAA GGC AGU CAU CUC CAG GUG GAG A. All siRNAs were synthesized by Invitrogen as Stealths, except for EB1 and FAM123A#1. Expression constructs were transiently transfected into HEK293T cells with Lipofectamine 2000 (Invitrogen Carlsbad, CA) or into HeLa cells with Fugene6-HD (Roche, Indianapolis, IN), as directed by the manufacturer. For gain-of-function reporter assays, cells were seeded in 48-well plates prior to transfection with a Firefly luciferase reporter, *Renilla* luciferase control reporter and effector plasmids. Cells stably engineered with these reporters were employed for the loss-of-function experiments. Luciferase activity was quantitated with the Dual Glow Luciferase Assay System (Promega, Madion, WI).

Affinity purification and mass spectrometry

Tandem affinity purification of FAM123A (isoform2) was performed as previously described (55, 56), with minor modifications. Protein complexes were eluted from the streptavidin beads with 5 mM biotin in the absence of TEV protease. 0.1% PPS Silent Surfactant (Protein Discovery, San Diego, CA) was included in the final elution from the calmodulin beads. Prior to mass spectrometry, PPS was acid cleaved at 37°C for 30 min. Flag-based AP/MS of FAM123C was performed in triplicate as previously described (57). Quantitative IP/MS of endogenous GEF-H1 was performed in duplicate via SILAC (K6/R10) labeling. Briefly, ~150mg of protein lysate from the following HEK293T-derived cell lines were compared at low confluency: parental cells (light) and Flag-FAM123A (heavy) or GFP (light) and HA-FAM123A (heavy). Cells were lysed in 50 mM Hepes-NaOH at pH 8.0, 150 mMNaCl, 10% glycerol, 0.1% NP40, 2 mM EDTA, 2 mM DTT, protease and phosphatase inhibitor cocktails (Roche, Indianapolis, IN) and subjected to immunoprecipitation with 10μg GEF-H1 antibody (A301-929A, Bethyl Labs, Montgomery, TX). Following an on-beads digestion with FASP Protein Digestion Kit (Protein Discovery, San Diego, CA), tryptic peptides were cleaned up by C18 Spin Column (Thermo Scientific, Waltham, MA), then separated by reverse phase nano-HPLC using a nanoAquity UPLC system (Waters Corp, Milford, MA). Peptides were first trapped in a 2 cm trapping column

(75 μm ID, Michrom Magic C18 beads of 5.0 μM particle size, 200 Å pore size) and then separated on a self-packed 25 cm column (75 μm ID, Michrom Magic C18 beads of 3.0 μM particle size, 100 Å pore size) at room temperature. The flow rate was 200 nl/min over a gradient of 1% buffer B (0.1% formic acid in acetonitrile) to 30% buffer B in 180 min. Then a following wash raised buffer B to 70%. The identity of the eluted peptides was determined with an in-line LTQ-Orbitrap Velos mass spectrometer (Thermo Scientific, Waltham, MA). The ion source was operated at 2.0-2.4 kV with ion transfer tube temperature set at 275 °C. Full MS scan (300-2000 m/z) was acquired in Orbitrap with 60,000 resolution setting, data-dependent MS^2 spectra were acquired in LTQ by collision induced dissociation (CID) using the 20 most intense ions. Precursor ions were selected based on charge states (1, 2 or 3) and intensity thresholds (above 2000) from the full scan, dynamic exclusion (one repeat during 30-s, a 60-s exclusion time window) was also taken into account. The polysiloxane lock mass of 445.120030 was used throughout spectral acquisition.

Protein identification and quantification

All raw data were converted to mzXML format before a search of the resultant spectra using Sorcerer™-SEQUEST® (build 4.0.4, Sage N Research, Milpitas, CA) and the Transproteomic Pipeline (TPP v4.3.1). Data were searched against the human UniProtKB/Swiss-Prot sequence database (Release 2011_08) supplemented with common contaminants, such as porcine (Swiss-Prot P00761) and bovine (P00760) trypsin, and further concatenated with its reversed copy as a decoy (40, 494 total sequences). Search parameters used were a precursor mass between 400 and 4500 amu, up to 2 missed cleavages, precursor-ion tolerance of 3 amu, accurate mass binning within Peptide Prophet (58), semi-tryptic digestion, a static carbamidomethyl cysteine modification, variable methionine oxidation, and additional variable modifications of R10 and K6 for SILAC experiments. SILAC ratios were calculated using TPP's XPRESS (59) and protein abundance ratios were first normalized by the bait's ratio, then combined from replicate experiments by taking a weighted average using the number of quantified spectra for the protein in each replicate. False discovery rates (FDR) were determined by ProteinProphet (58) and minimum protein probability cutoffs resulting in a 1% FDR were selected individually for each experiment. Further filtering of identified proteins was accomplished using the following criteria: at least 2 unique peptides were identified for the protein in each of at least 2 (out of 4) WTX experiments, at least 2 (out of 3) for proteins in FAM123C experiments, 2 (out of 2) for ARHGEF2, and 2 (out of 3) for FAM123A. Common contaminants were removed at the authors' discretion based on previous experiments, such as keratins, ribosomal, and DEAD box proteins. Unfiltered data are provided as Table S1 and may be downloaded from ProteomeCommons.org Tranche using the following hash: SG+Lb +X7PAOmf9pdlyQREvVmA7sOZX/ iwKCV7zQBvmofGaBNxvXg8D9dZkUs5CgbiDMIBp6JlNW1fh0EgeWb8SOaaxMAAAA AAAADcA==

Bioinformatics

PeptideProphet/ProteinProphet results for each AP-MS experiment were stored in a local Prohits database (60). Prohits performed the mapping of UniProtKB accession identifiers to Entrez Gene IDs. These results were then imported into Cytoscape v2.8.2 (61) for network visualization. Gene Ontology annotations were imported from NCBI Entrez Gene through Cytoscape. Known protein-protein interactions were extracted from the following databases: BIND, BioGRID, DIP, HPRD, IntAct, MINT, and Reactome – downloaded on 08/15/2010.

Affinity pull-downs, Immunoprecipitation, and Western blotting

In all biochemical experiments cells were lysed in a buffer containing 50 mM Tris-HCl at pH 8.0, 150 mM NaCl, 10% glycerol, 1% TritonX-100, 2 mM EDTA, protease and

phosphatase inhibitor cocktails (Roche). For streptavidin affinity purification cleared lysates were incubated 1 hour with streptavidin resin (GE Healthcare, Piscataway, NJ) before washing and eluting. Immunoprecipitation of endogenous GEF-H1 was performed using antibodies anti-GEF-H1 (A301-929A, Bethyl Labs, Montgomery, TX). Detection of proteins by Western blot was performed using the following antibodies: anti-FLAG M2 monoclonal (Sigma-Aldrich Corporation, St. Louis, MO); anti-HA polyclonal (1867423; Roche, Indianapolis, IN; anti-GFP polyclonal (ab290, Abcam, Cambridge, MA); anti-β-catenin polyclonal (9562; Cell Signaling Technology, Danvers, MA); anti-βTrCP1 monoclonal (37-3400, Invitrogen Carlsbad, CA); anti β-tubulin monoclonal (T7816; Sigma-Aldrich Corporation, St. Louis, MO); anti-GEF-H1 (A301-928A, Bethyl Labs, Montgomery, TX); anti-MARK2 (Roche, Indianapolis, IN); anti-CLASP2 (A302-155A, Bethyl Labs, Montgomery, TX); anti-APC polyclonal (A300-180A, A300-981A, Bethyl Labs, Montgomery, TX); and anti-EB1 monoclonal (610534, BD Transduction Laboratories, Franklin Lakes, NJ); anti-MLC2 (3672, Cell Signaling Technology, Danvers, MA); anti-p-MLC2 Ser19 (#3671, Cell Signaling Technology, Danvers, MA). To detect endogenous FAM123A, a custom monoclonal antibody was produced (Abmart, Shanghai, China).

For phospho-MLC detection, Hela cells were transfected with siRNA at 10nM for 48h. Cells were lysed in the well with UPX sample buffer from Protein Discovery (San Diego, CA) supplemented with protease and phosphatase inhibitors. Samples were boiled for 3 min before addition of 4× sample buffer and sonication. Proteins were detected by Western blot and quantified using Odyssey Imager and Software by LiCor Biosciences (Lincoln, NE).

Immunofluorescence

For immunofluorescence, HeLa sarcoma cells were plated on 10ug/ml fibronectin-coated coverslips in Dulbecco's modified Eagle's medium (DMEM) supplemented with 10% fetal bovine serum and allowed to attach and spread. Cells were fixed in 4% paraformaldehyde (PFA, Electron Microscopy Sciences, Hatfield, PA) in cytoskeletal buffer (CS; 5 mM PIPES, pH 6, 137 mM NaCl, 5 mM KCl, 1.1 mM Na2HPO4, 0.4 mM KH2PO4, 0.4 mM MgCl2, 0.4 mM NaHCO3, 2 mM EGTA, 50mM glucose) for 15 min, and permeabilized with 0.1% Triton in phosphate buffer saline (PBS) for 5 min. After blocking in 1% bovine serum albumin (BSA)/PBS for 1hour, cells were incubated with primary antibodies at 4C, overnight, followed by incubation with appropriate secondary antibodies RRX-conjugated-donkey anti-mouse IgG and FITC-conjugated-donkey anti-mouse IgG (Jackson ImmunoResearch Laboratories, West Grove, PA) at room temperature for 1 hour. For staining of endogenous EB1, cells were fixed in methanol at -20C for 5 min. Staining of proteins was performed using the following antibodies: monoclonal anti-α-tubulin (clone DM1A, T9026, Sigma-Aldrich Corporation, St. Louis, MO), monoclonal anti-vinculin (clone nVIN-1, V9131, Sigma-Aldrich Corporation, St. Louis, MO) and anti-EB1 monoclonal (610534, BD Transduction Laboratories, Franklin Lakes, NJ). Actin was stained using Alexa Fluor 647-phalloidin or Alexa Fluor 594-phalloidin (Invitrogen Carlsbad, CA). Coverslips were mounted to slides using the Prolong Gold antifade reagent (Invitrogen Carlsbad, CA). Staining was analyzed using an Olympus IX 81-ZDC Inverted Fluorescence Microscope (Olympus Corporation of the Americas, Center Valley, PA) equipped with a 60X/1.42 Oil PlanApo objective lenses and a Hamamatsu C10600-10B camera (OrcaR2, Hamamatsu Photonics LTD, Japan).

For subcellular localization of FAM123A, HeLa cells were grown on 18-mm glass coverslips coated with Poly-L-Lysine (Sigma-Aldrich Corporation, St. Louis, MO) and co-transfected with EGFP-FAM123A and cherry-tubulin. Cells were in fixed in 1% paraformaldehyde in pure -20°C Methanol for 2 min and mounted using Prolog antifade gold with DAPI (Invitrogen Carlsbad, CA). The imaging was performed on a Deltavision deconvolution microscope (Applied Precision, Issaquah WA). To co-stain FAM123A-GFP

and EB1, cells were fixed similarly and EB1 was stained with anti-EB1antibody (BD Transduction Laboratories, Franklin Lakes, NJ), followed by incubation with Donkey anti-mouse secondary (Jackson ImmunoResearch Laboratories, West Grove, PA). Fixed cells were imaged with a complete Z-series in 0.2 micron sections, deconvolved and projected using Adobe Photoshop CS and Image J software.

For comparing the distribution of FAM123A family members, HEK293T transiently expressing fluorescent-tagged proteins were plated on fibronectin coated coverslips, fixed and mounted as described above and imaged using a Zeiss LSM5 Pascal Confocal Laser Scanning Microscope equipped with a 63X/1.42 Oil PlanApo objective lenses.

Live cell imaging

For low resolution imaging analysis, HT1080 sarcoma cells were plated onto 5ug/ml fibronectin-coated Mattek dishes (Mattek Corporation, Ashland, MA) in Dulbecco's modified Eagle's medium (DMEM) supplemented with 10% fetal bovine serum and allowed to attach and spread. Cells were transfected with venus-FAM123A or venus-WTX using Fugene HD (Promega, Madison, WI) according to manufacturer's instructions. Cells were imaged the next day in contrast phase and GFP fluorescence on a Nikon Biostation (every 5 min for 10 hours, Nikon, Belmont, CA), with a 20x objective, while at 37°C and 5% CO_2.

For dynamic analysis of fluorescence–tagged proteins at higher magnification, HT1080 were plated onto 5ug/ml fibronectin coated Delta T dishes (Bioptechs, Inc, Butler, PA) in Dulbecco's modified Eagle's medium (DMEM) supplemented with 10% fetal bovine serum and transfected with EGFP-FAM123A using Fugene HD (Promega, Madison, WI). Next day cells were imaged at 37°C and 5% CO_2, using an Olympus IX 81-ZDC Inverted Fluorescence Microscope (Olympus Corporation of the Americas, Center Valley, PA) equipped with a Bioptechs Delta T Open Dish System (Bioptechs, Inc, Butler, PA) with a heated lid. Time lapse images were captured every 10 seconds, using a heated 60X/1.42 Oil PlanApo objective lenses and a Hamamatsu C10600-10B camera (OrcaR2, Hamamatsu Photonics LTD, Japan). Data acquisition was carried out using Volocity (version 5.5.1, PerkinElmer), and image processing was performed using ImageJ and Adobe Photoshop CS software.

HeLa cells were transfected with either EGFP-FAM123A, and EGFP-C-terminus FAM123A or EGFP-C-terminus-FAM123A-IPAA and in some cases co-transfected with EB3-RFP using a Nucleofector-II (Amaxa Biosystems, Gaithersburg, MD) and plated onto Poly-D-lysine coated MatTek dishes. After 24 hours of expression the dually-transfected cells were imaged at 37°C at a rate of 1 frame/5s. on a Deltavision-RT microscope (Applied Precision, Issaquah, WA). Cells transfected with only one construct (movie S6 and movie S7) were imaged at a rate of 1 frame/2s.

For microtubule dynamic studies, HeLa cells were transfected with EB3-GFP and RFP-Utr expressing DNA constructs and plated onto fibronectin coated MatTek filming dishes; RFP-Utr encodes an RFP-fused calponin homology domain of the utrophin protein (62). The cells were transfected for 48 hours with either control siRNA or siRNA directed against FAM123A. The cells were then imaged using a Personal Deltavision (L.W.) custom outfitted with TIRF light paths and a 60× Olympus TIRF objective. Images were collected at 5 second intervals. Z-projections were made using successive 5-frame intervals for a total of 15 frames. Each 5 frame projection was colored red, green or blue to visualize the assembling microtubule ends. Using this regime, stationary microtubule ends consisting of RGB overlap are depicted as white.

To quantitate cell migration, HeLa cells were transfected with 10 nM siRNA and plated onto a 12 well plate ($4\times10e^5$ cells/well) in complete growth media 48 hours after transfections. After 12 hours, the monolayer of cells were wounded by manual scratching with a pipet tip, washed with PBS and placed into complete growth medium. Time lapse phase contrast images were acquired every 7 min for 18h using an Olympus I×70 Inverted Fluorescence Microscope, enclosed within an environmental chamber controlling temperature, relative humidity and CO2, and equipped with a 4× 0.13 Uplan FL PhL lens and a Hamamatasu ORCA C4742-95 CCD camera. Data was acquired with Velocity (version 5.5.1, PerkinElmer). To calculate relative migration, the scratch area was determined from movie-derived images at time zero and at 6 hours. The difference in area between t=0 and t=6 at 3 locations along the scratch for each of the biological triplicate experiments was used to plot the relative rate of wound closure.

RhoA and GEF-H1 activity assays

Purified GST-RhoA(G17A) was kindly provided Christophe Guilluy and Keith Burridge (UNC Chapel Hill, USA). Affinity precipitation of exchange factors with the nucleotide-free RhoA mutant (G17A) was performed as previously described (28). For quantitation, Western blot data from 6 biological replicate experiments were analyzed by densitometry. Data were first normalized to a loading control and then to 1 before averaging and plotting. Paired Students *t* Test was calculated using raw data. For RhoA activity quantitation, the G-LISA RhoA Activation Assay Biochem Kit (Cytoskeleton Inc., Denver, CO) was employed. Specifically, 4×10^5 Hela cells were plated in 60mM plates. Cells were transfected overnight with siRNA and allowed to recover in 10% FBS DMEM for 8 hours. Cells were then washed with PBS and starved in DMEM for 48 hours with 1 media change at 24 hours. After 1 hour treatment with nocodazole, cells were lysed in 140μl of cell lysis buffer. Plates were read on Synergy HT microplate reader from Biotek (Winooski, VT).

Cell Adhesion and Spreading assay

Cell adhesion and spreading were measured as changes in impedance using the RT-CES system (ACEABiosciences Inc. San Diego, CA). The 16-well E-plates were coated with 10μg/ml fibronectin for 1 hour at 37°C. HeLa cells were transfected with 10nM siRNAs and subjected to cell spreading assay approximately 65 hours after transfection. For measurements, the same number of cells (4×10^3) was added to each well. The e-plates containing HeLas were allowed to incubate at room temperature for 10 min before being placed on the device station in the incubator for continuous recording of impedance-based cell index (CI; every 30 seconds, for 3 hours). Additionally, siRNA-transfected cells were plated on fibronectin coated coverslips, allowed to attach and spread for various periods of time, fixed and stained for vinculin according to methods described above.

Supplementary Material

Refer to Web version on PubMed Central for supplementary material.

Acknowledgments

We are grateful to Randall T. Moon and the members of Moon laboratory and Major laboratory for their invaluable assistance. We also thank Randall T. Moon and the Howard Hughes Medical Institute for providing space and funding for M. Motolese during the early stages of this work. We additionally thank Ferdinando Nicoletti for financial support to M. Motolese. We thank Anna Akhmanova, Christophe Guilluy and Natalia Mitin for helpful advice.

Funding: M.B.M. is supported by the National Institutes of Health through the NIH Director's New Innovator Award, 1-DP2-OD007149-01 and a Scholar Award from the Sidney Kimmel Cancer Foundation. L.W. is supported by GM69429/GM/NIGMS from the National Institutes of Health.

References

1. Rivera MN, Kim WJ, Wells J, Driscoll DR, Brannigan BW, Han M, Kim JC, Feinberg AP, Gerald WL, Vargas SO, Chin L, Iafrate AJ, Bell DW, Haber DA. An X chromosome gene, WTX, is commonly inactivated in Wilms tumor. Science. 2007; 315:642–645. [PubMed: 17204608]
2. Ruteshouser EC, Robinson SM, Huff V. Wilms tumor genetics: mutations in WT1, WTX, and CTNNB1 account for only about one-third of tumors. Genes Chromosomes Cancer. 2008; 47:461–470. [PubMed: 18311776]
3. Jenkins ZA, van Kogelenberg M, Morgan T, Jeffs A, Fukuzawa R, Pearl E, Thaller C, Hing AV, Porteous ME, Garcia-Minaur S, Bohring A, Lacombe D, Stewart F, Fiskerstrand T, Bindoff L, Berland S, Ades LC, Tchan M, David A, Wilson LC, Hennekam RC, Donnai D, Mansour S, Cormier-Daire V, Robertson SP. Germline mutations in WTX cause a sclerosing skeletal dysplasia but do not predispose to tumorigenesis. Nat Genet. 2009; 41:95–100. [PubMed: 19079258]
4. Moisan A, Rivera MN, Lotinun S, Akhavanfard S, Coffman EJ, Cook EB, Stoykova S, Mukherjee S, Schoonmaker JA, Burger A, Kim WJ, Kronenberg HM, Baron R, Haber DA, Bardeesy N. The WTX tumor suppressor regulates mesenchymal progenitor cell fate specification. Dev Cell. 2011; 20:583–596. [PubMed: 21571217]
5. Major MB, Camp ND, Berndt JD, Yi X, Goldenberg SJ, Hubbert C, Biechele TL, Gingras AC, Zheng N, Maccoss MJ, Angers S, Moon RT. Wilms tumor suppressor WTX negatively regulates WNT/beta-catenin signaling. Science. 2007; 316:1043–1046. [PubMed: 17510365]
6. Grohmann A, Tanneberger K, Alzner A, Schneikert J, Behrens J. AMER1 regulates the distribution of the tumor suppressor APC between microtubules and the plasma membrane. J Cell Sci. 2007; 120:3738–3747. [PubMed: 17925383]
7. Tanneberger K, Pfister AS, Kriz V, Bryja V, Schambony A, Behrens J. Structural and functional characterization of the Wnt inhibitor APC membrane recruitment 1 (Amer1). J Biol Chem. 2011; 286:19204–19214. [PubMed: 21498506]
8. Tanneberger K, Pfister AS, Brauburger K, Schneikert J, Hadjihannas MV, Kriz V, Schulte G, Bryja V, Behrens J. Amer1/WTX couples Wnt-induced formation of PtdIns(4,5) P2 to LRP6 phosphorylation. The EMBO journal. 2011; 30:1433–1443. [PubMed: 21304492]
9. Boutet A, Comai G, Schedl A. The WTX/AMER1 gene family: evolution, signature and function. BMC Evol Biol. 2010; 10:280. [PubMed: 20843316]
10. Comai G, Boutet A, Neirijnck Y, Schedl A. Expression patterns of the Wtx/Amer gene family during mouse embryonic development. Dev Dyn. 2010; 239:1867–1878. [PubMed: 20503382]
11. Pfister AS, Tanneberger K, Schambony A, Behrens J. Amer2 is a novel negative regulator of Wnt/beta-catenin signaling involved in neuroectodermal patterning. J Biol Chem. 2011
12. Vaughan KT. TIP maker and TIP marker; EB1 as a master controller of microtubule plus ends. The Journal of cell biology. 2005; 171:197–200. [PubMed: 16247021]
13. Bieling P, Kandels-Lewis S, Telley IA, van Dijk J, Janke C, Surrey T. CLIP-170 tracks growing microtubule ends by dynamically recognizing composite EB1/tubulin-binding sites. The Journal of cell biology. 2008; 183:1223–1233. [PubMed: 19103809]
14. Vitre B, Coquelle FM, Heichette C, Garnier C, Chretien D, Arnal I. EB1 regulates microtubule dynamics and tubulin sheet closure in vitro. Nature cell biology. 2008; 10:415–421.
15. Kaverina I, Straube A. Regulation of cell migration by dynamic microtubules. Semin Cell Dev Biol. 2011; 22:968–974. [PubMed: 22001384]
16. van der Vaart B, Akhmanova A, Straube A. Regulation of microtubule dynamic instability. Biochem Soc Trans. 2009; 37:1007–1013. [PubMed: 19754441]
17. Akhmanova A, Steinmetz MO. Tracking the ends: a dynamic protein network controls the fate of microtubule tips. Nat Rev Mol Cell Biol. 2008; 9:309–322. [PubMed: 18322465]
18. Wu X, Kodama A, Fuchs E. ACF7 regulates cytoskeletal-focal adhesion dynamics and migration and has ATPase activity. Cell. 2008; 135:137–148. [PubMed: 18854161]
19. Akhmanova A, Steinmetz MO. Microtubule +TIPs at a glance. J Cell Sci. 2010; 123:3415–3419. [PubMed: 20930136]
20. Kodama A, Karakesisoglou I, Wong E, Vaezi A, Fuchs E. ACF7: an essential integrator of microtubule dynamics. Cell. 2003; 115:343–354. [PubMed: 14636561]

21. Su LK, Burrell M, Hill DE, Gyuris J, Brent R, Wiltshire R, Trent J, Vogelstein B, Kinzler KW. APC binds to the novel protein EB1. Cancer Res. 1995; 55:2972–2977. [PubMed: 7606712]
22. Honnappa S, Gouveia SM, Weisbrich A, Damberger FF, Bhavesh NS, Jawhari H, Grigoriev I, van Rijssel FJ, Buey RM, Lawera A, Jelesarov I, Winkler FK, Wuthrich K, Akhmanova A, Steinmetz MO. An EB1-binding motif acts as a microtubule tip localization signal. Cell. 2009; 138:366–376. [PubMed: 19632184]
23. Li R, Gundersen GG. Beyond polymer polarity: how the cytoskeleton builds a polarized cell. Nat Rev Mol Cell Biol. 2008; 9:860–873. [PubMed: 18946475]
24. Chang YC, Nalbant P, Birkenfeld J, Chang ZF, Bokoch GM. GEF-H1 couples nocodazole-induced microtubule disassembly to cell contractility via RhoA. Mol Biol Cell. 2008; 19:2147–2153. [PubMed: 18287519]
25. Krendel M, Zenke FT, Bokoch GM. Nucleotide exchange factor GEF-H1 mediates cross-talk between microtubules and the actin cytoskeleton. Nature cell biology. 2002; 4:294–301.
26. Uehata M, Ishizaki T, Satoh H, Ono T, Kawahara T, Morishita T, Tamakawa H, Yamagami K, Inui J, Maekawa M, Narumiya S. Calcium sensitization of smooth muscle mediated by a Rho-associated protein kinase in hypertension. Nature. 1997; 389:990–994. [PubMed: 9353125]
27. Hill CS, Wynne J, Treisman R. The Rho family GTPases RhoA, Rac1, and CDC42Hs regulate transcriptional activation by SRF. Cell. 1995; 81:1159–1170. [PubMed: 7600583]
28. Garcia-Mata R, Wennerberg K, Arthur WT, Noren NK, Ellerbroek SM, Burridge K. Analysis of activated GAPs and GEFs in cell lysates. Methods in enzymology. 2006; 406:425–437. [PubMed: 16472675]
29. Hatanaka H, Ogura K, Moriyama K, Ichikawa S, Yahara I, Inagaki F. Tertiary structure of destrin and structural similarity between two actin-regulating protein families. Cell. 1996; 85:1047–1055. [PubMed: 8674111]
30. Moriyama K, Nishida E, Yonezawa N, Sakai H, Matsumoto S, Iida K, Yahara I. Destrin, a mammalian actin-depolymerizing protein, is closely related to cofilin. Cloning and expression of porcine brain destrin cDNA. J Biol Chem. 1990; 265:5768–5773. [PubMed: 2156828]
31. Storbeck CJ, Wagner S, O'Reilly P, McKay M, Parks RJ, Westphal H, Sabourin LA. The Ldb1 and Ldb2 transcriptional cofactors interact with the Ste20-like kinase SLK and regulate cell migration. Mol Biol Cell. 2009; 20:4174–4182. [PubMed: 19675209]
32. Burakov AV, Zhapparova ON, Kovalenko OV, Zinovkina LA, Potekhina ES, Shanina NA, Weiss DG, Kuznetsov SA, Nadezhdina ES. Ste20-related protein kinase LOSK (SLK) controls microtubule radial array in interphase. Mol Biol Cell. 2008; 19:1952–1961. [PubMed: 18287541]
33. Wagner S, Flood TA, O'Reilly P, Hume K, Sabourin LA. Association of the Ste20-like kinase (SLK) with the microtubule. Role in Rac1-mediated regulation of actin dynamics during cell adhesion and spreading. J Biol Chem. 2002; 277:37685–37692. [PubMed: 12151406]
34. Leopoldt D, Yee HF Jr, Rozengurt E. Calyculin-A induces focal adhesion assembly and tyrosine phosphorylation of p125(Fak), p130(Cas), and paxillin in Swiss 3T3 cells. Journal of cellular physiology. 2001; 188:106–119. [PubMed: 11382927]
35. Riveline D, Zamir E, Balaban NQ, Schwarz US, Ishizaki T, Narumiya S, Kam Z, Geiger B, Bershadsky AD. Focal contacts as mechanosensors: externally applied local mechanical force induces growth of focal contacts by an mDia1-dependent and ROCK-independent mechanism. The Journal of cell biology. 2001; 153:1175–1186. [PubMed: 11402062]
36. Schuyler SC, Pellman D. Microtubule “plus-end-tracking proteins”: The end is just the beginning. Cell. 2001; 105:421–424. [PubMed: 11371339]
37. Akhmanova A, Hoogenraad CC, Drabek K, Stepanova T, Dortland B, Verkerk T, Vermeulen W, Burgering BM, De Zeeuw CI, Grosveld F, Galjart N. Clasps are CLIP-115 and -170 associating proteins involved in the regional regulation of microtubule dynamics in motile fibroblasts. Cell. 2001; 104:923–935. [PubMed: 11290329]
38. Nathke IS, Adams CL, Polakis P, Sellin JH, Nelson WJ. The adenomatous polyposis coli tumor suppressor protein localizes to plasma membrane sites involved in active cell migration. The Journal of cell biology. 1996; 134:165–179. [PubMed: 8698812]
39. Bienz M. The subcellular destinations of APC proteins. Nat Rev Mol Cell Biol. 2002; 3:328–338. [PubMed: 11988767]

40. Fong KW, Hau SY, Kho YS, Jia Y, He L, Qi RZ. Interaction of CDK5RAP2 with EB1 to track growing microtubule tips and to regulate microtubule dynamics. Mol Biol Cell. 2009; 20:3660–3670. [PubMed: 19553473]
41. Drabek K, van Ham M, Stepanova T, Draegestein K, van Horssen R, Sayas CL, Akhmanova A, Ten Hagen T, Smits R, Fodde R, Grosveld F, Galjart N. Role of CLASP2 in microtubule stabilization and the regulation of persistent motility. Current biology: CB. 2006; 16:2259–2264. [PubMed: 17113391]
42. Wen Y, Eng CH, Schmoranzer J, Cabrera-Poch N, Morris EJ, Chen M, Wallar BJ, Alberts AS, Gundersen GG. EB1 and APC bind to mDia to stabilize microtubules downstream of Rho and promote cell migration. Nature cell biology. 2004; 6:820–830.
43. Logue JS, Whiting JL, Tunquist B, Sacks DB, Langeberg LK, Wordeman L, Scott JD. AKAP220 protein organizes signaling elements that impact cell migration. J Biol Chem. 2011; 286:39269–39281. [PubMed: 21890631]
44. Myers KA, Applegate KT, Danuser G, Fischer RS, Waterman CM. Distinct ECM mechanosensing pathways regulate microtubule dynamics to control endothelial cell branching morphogenesis. The Journal of cell biology. 2011; 192:321–334. [PubMed: 21263030]
45. Birkenfeld J, Nalbant P, Bohl BP, Pertz O, Hahn KM, Bokoch GM. GEF-H1 modulates localized RhoA activation during cytokinesis under the control of mitotic kinases. Dev Cell. 2007; 12:699–712. [PubMed: 17488622]
46. Callow MG, Zozulya S, Gishizky ML, Jallal B, Smeal T. PAK4 mediates morphological changes through the regulation of GEF-H1. J Cell Sci. 2005; 118:1861–1872. [PubMed: 15827085]
47. Fujishiro SH, Tanimura S, Mure S, Kashimoto Y, Watanabe K, Kohno M. ERK1/2 phosphorylate GEF-H1 to enhance its guanine nucleotide exchange activity toward RhoA. Biochem Biophys Res Commun. 2008; 368:162–167. [PubMed: 18211802]
48. Kakiashvili E, Dan Q, Vandermeer M, Zhang Y, Waheed F, Pham M, Szaszi K. The epidermal growth factor receptor mediates tumor necrosis factor-alpha-induced activation of the ERK/GEF-H1/RhoA pathway in tubular epithelium. J Biol Chem. 2011; 286:9268–9279. [PubMed: 21212278]
49. Kakiashvili E, Speight P, Waheed F, Seth R, Lodyga M, Tanimura S, Kohno M, Rotstein OD, Kapus A, Szaszi K. GEF-H1 mediates tumor necrosis factor-alpha-induced Rho activation and myosin phosphorylation: role in the regulation of tubular paracellular permeability. J Biol Chem. 2009; 284:11454–11466. [PubMed: 19261619]
50. Matsuzawa T, Kuwae A, Yoshida S, Sasakawa C, Abe A. Enteropathogenic Escherichia coli activates the RhoA signaling pathway via the stimulation of GEF-H1. The EMBO journal. 2004; 23:3570–3582. [PubMed: 15318166]
51. Tonami K, Kurihara Y, Arima S, Nishiyama K, Uchijima Y, Asano T, Sorimachi H, Kurihara H. Calpain-6, a microtubule-stabilizing protein, regulates Rac1 activity and cell motility through interaction with GEF-H1. J Cell Sci. 2011; 124:1214–1223. [PubMed: 21406564]
52. Yamahashi Y, Saito Y, Murata-Kamiya N, Hatakeyama M. Polarity-regulating Kinase Partitioning-defective 1b (PAR1b) Phosphorylates Guanine Nucleotide Exchange Factor H1 (GEF-H1) to Regulate RhoA-dependent Actin Cytoskeletal Reorganization. J Biol Chem. 2011; 286:44576–44584. [PubMed: 22072711]
53. Yoshimura Y, Miki H. Dynamic regulation of GEF-H1 localization at microtubules by Par1b/MARK2. Biochem Biophys Res Commun. 2011; 408:322–328. [PubMed: 21513698]
54. Zenke FT, Krendel M, DerMardirossian C, King CC, Bohl BP, Bokoch GM. p21-activated kinase 1 phosphorylates and regulates 14-3-3 binding to GEF-H1, a microtubule-localized Rho exchange factor. J Biol Chem. 2004; 279:18392–18400. [PubMed: 14970201]
55. Angers S. Proteomic analyses of protein complexes in the Wnt pathway. Methods Mol Biol. 2008; 468:223–230. [PubMed: 19099258]
56. Angers S, Thorpe CJ, Biechele TL, Goldenberg SJ, Zheng N, MacCoss MJ, Moon RT. The KLHL12-Cullin-3 ubiquitin ligase negatively regulates the Wnt-beta-catenin pathway by targeting Dishevelled for degradation. Nature cell biology. 2006; 8:348–357.
57. Chen GI, Gingras AC. Affinity-purification mass spectrometry (AP-MS) of serine/threonine phosphatases. Methods. 2007; 42:298–305. [PubMed: 17532517]

58. Keller A, Nesvizhskii AI, Kolker E, Aebersold R. Empirical statistical model to estimate the accuracy of peptide identifications made by MS/MS and database search. Analytical chemistry. 2002; 74:5383–5392. [PubMed: 12403597]

59. Han DK, Eng J, Zhou H, Aebersold R. Quantitative profiling of differentiation-induced microsomal proteins using isotope-coded affinity tags and mass spectrometry. Nat Biotechnol. 2001; 19:946–951. [PubMed: 11581660]

60. Liu G, Zhang J, Larsen B, Stark C, Breitkreutz A, Lin ZY, Breitkreutz BJ, Ding Y, Colwill K, Pasculescu A, Pawson T, Wrana JL, Nesvizhskii AI, Raught B, Tyers M, Gingras AC. ProHits: integrated software for mass spectrometry-based interaction proteomics. Nat Biotechnol. 2010; 28:1015–1017. [PubMed: 20944583]

61. Smoot ME, Ono K, Ruscheinski J, Wang PL, Ideker T. Cytoscape 2.8: new features for data integration and network visualization. Bioinformatics. 2011; 27:431–432. [PubMed: 21149340]

62. Burkel BM, von Dassow G, Bement WM. Versatile fluorescent probes for actin filaments based on the actin-binding domain of utrophin. Cell Motil Cytoskeleton. 2007; 64:822–832. [PubMed: 17685442]

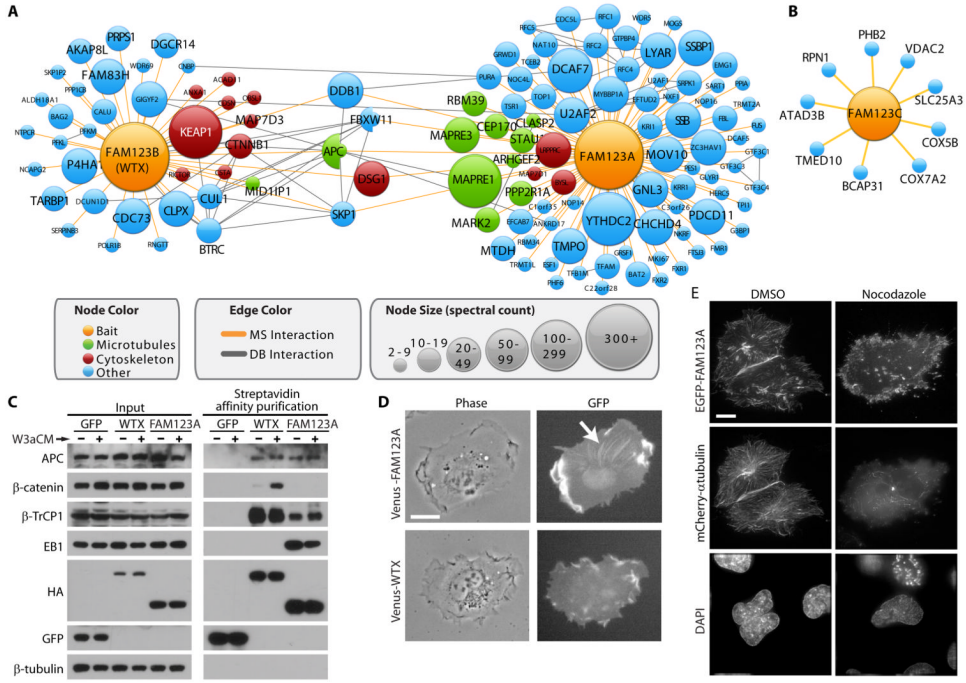

Figure 1. FAM123A associates with a microtubule enriched protein interaction network and moves on microtubules

(A) The WTX and FAM123A protein interaction networks as defined by affinity purification and mass spectrometry. Proteins shown were represented by at least 2 unique peptides in at least 2 (out of 4) WTX experiments or at least 2 (out of 3) in FAM123A experiments. DB, database. **(B)** The FAM123C protein interaction network, as defined by proteins which were identified by at least 2 independent peptides in at least 2 out of 3 experiments. In (A) and (B), node size and coloring reflects spectral counts and gene ontology, respectively. **(C)** Streptavidin affinity purified protein complexes from HEK293T cells stably expressing SBPHA-GFP, SBPHA-WTX or SBPHA-FAM123A were analyzed by Western blot for the indicated endogenous proteins (SBP, streptavidin binding peptide; HA, hemagglutinin). Data represent 2 biological replicates. **(D)** Images from movies of HT1080 cells that were transiently transfected with Venus-tagged FAM123A (movie S1) or WTX (movie S2) constructs. Data are representative of two independent biological replicates. Scale bar 20μm. **(E)** HeLa cells were transfected with EGFP-FAM123A and mCherry-tagged α-tubulin, treated with DMSO or nocadozole (NOC), fixed, and imaged by deconvolution microscopy. The FAM123A image is representative of five independent experiments imaged on five different days. Of 65 imaged cells 39 exhibited long filamentous structures in cells expressing FAM123A-Venus that co-localized with microtubules. Scale bar 5μm.

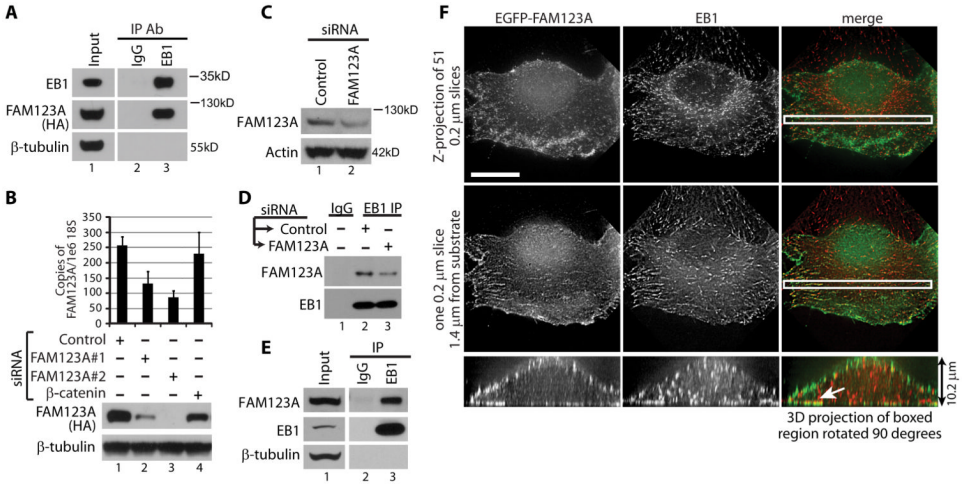

Figure 2. Interaction of FAM123A with EB1

(A) EB1 or anti-mouse immunoprecipitates from HEK293T cells stably expressing SBPHA-FAM123A were immunoblotted for the indicated proteins. Data represent 4 biological replicates. **(B)** Top: *FAM123A* mRNA quantitation by quantitative PCR of HEK293T cells transfected with the indicated siRNAs. The mRNA copy number of *FAM123A* was normalized to 18S ribosomal RNA. Error bars represent standard deviation in the PCR reactions. Bottom: Western blot analysis of FAM123A abundance in SBPHA-FAM123A stable HEK293T cells transfected with the indicated siRNAs. **(C)** Western blot analysis of endogenous FAM123A in HEK293T cells transfected with control or FAM123A-specific siRNA#2. **(D)** Endogenous EB1 protein complexes from HEK293T cells were immunoblotted for FAM123A. **(E)** Endogenous EB1 immunoprecipitates from HeLa cells were immunoblotted for FAM123A. **(F)** HeLa cells transfected with EGFP-FAM123A were fixed, stained for endogenous EB1, and imaged with confocal microscopy. A Z-projection for all captured 0.2 μM slices and a single 0.2μM slice at the bottom of the cell is shown. The co-localization of EGFP-FAM123A with EB1 was analyzed in two independent experiments imaged on two different days. For 20 EGFP-FAM123A cells analyzed, all 20 showed co-localization with EB1. Scale bar 10μm.

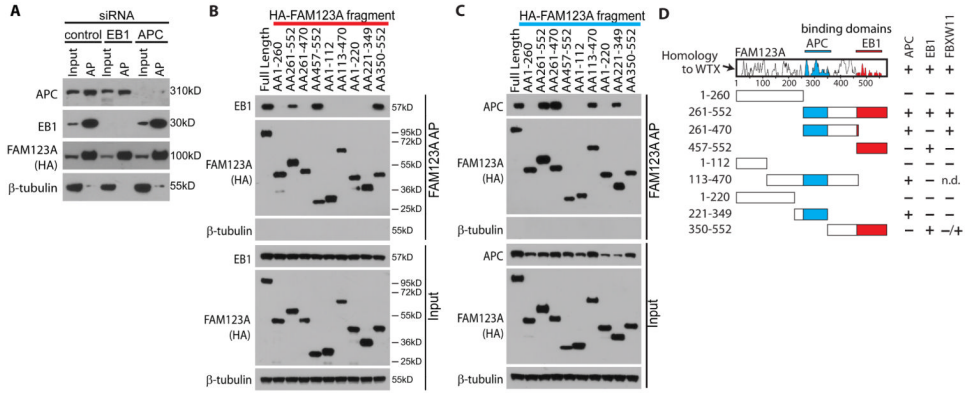

Figure 3. FAM123A binds APC and EB1 through distinct domains

(A) Cells stably expressing SBPHA-FAM123A were transiently transfected with the indicated siRNAs, lysed, subjected to streptavidin-affinity purification (AP), and Western blotted. **(B-C)** HEK293T cells transiently transfected with EB1-EGFP **(B)** or APC (AA1-1060) **(C)** and the indicated SBPHA-FAM123A fragment were lysed, subjected to streptavidin-affinity purification and Western blotted. Data represent 3 biological replicates. **(D)** The protein domain interaction mapping shown in B, C and Figure S2.

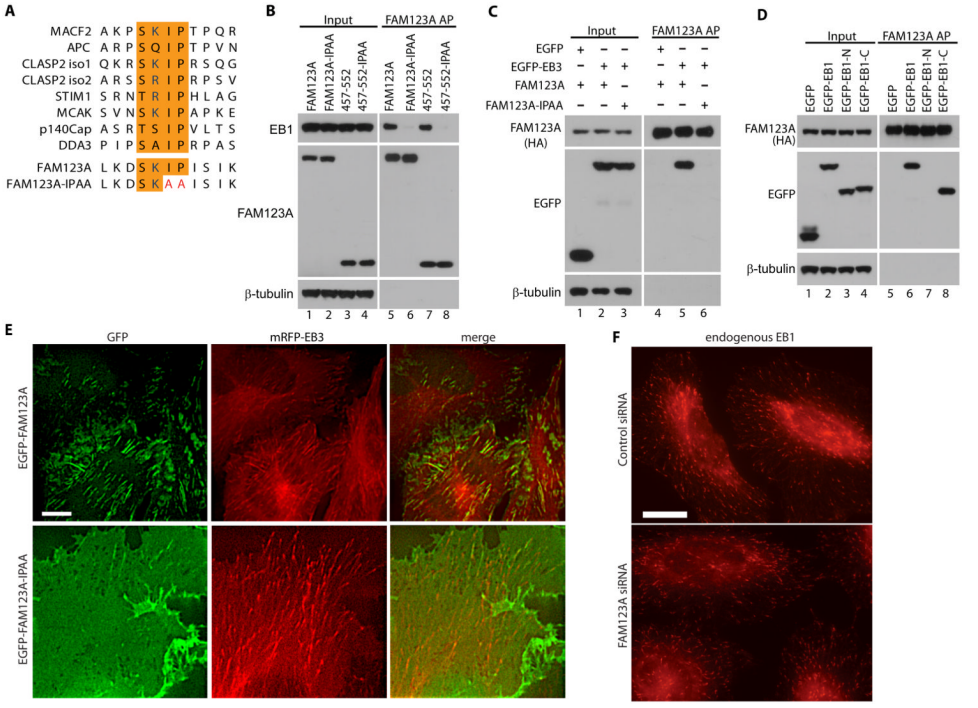

Figure 4. EB1-association is required for FAM123A microtubule localization

(A) Protein sequence alignment of FAM123A and the SxIP domains of various plus-end tracking proteins. **(B-C)** Western blot analysis of streptavidin-affinity pull-downs from HEK293T transfected with EB1-EGFP (B) or EB3-EGFP (C) and the indicated SBPHA-FAM123A constructs. Data represent 3 biological replicates. **(D)** Western blot analysis of streptavidin-affinity pull-downs assay followed by Western blot analysis of SBPHA-FAM123A cells transfected with EGFP, EB1-EGFP, EGFP-EB1-N or EGFP-EB1-C. Data represent 2 biological replicates. **(E)** Images from live cell imaging of HeLa cells expressing EGFP-FAM123A (movie S4) or EGFP-FAM123A-IPAA (movie S5). The co-localization of EGFP-FAM123A was compared to EGFP-FAM123A-IPAA in three replicate experiments imaged on three separate days. For EGFP-FAM123A a total of 37 cells were imaged live in conjunction with mRFP-EB3. All cells exhibited greater than or equal to 75% localization of EGFP-FAM123A with mRFP-EB3 in thresholded images. Of 15 EGFP-FAM123A-IPAA cells, no cell exhibited more than 5% co-localization of EGFP-FAM123A-IPAA with mRFP-EB3. Scale bar 5μm. **(F)** HeLa cells transfected with the indicated siRNAs were co-stained for EB1 and DAPI. EB1 staining is representative of two biological replicate in which 46 FAM123A depleted cells and 33 control siRNA transfected cells where imaged. Scale bar 20μm.

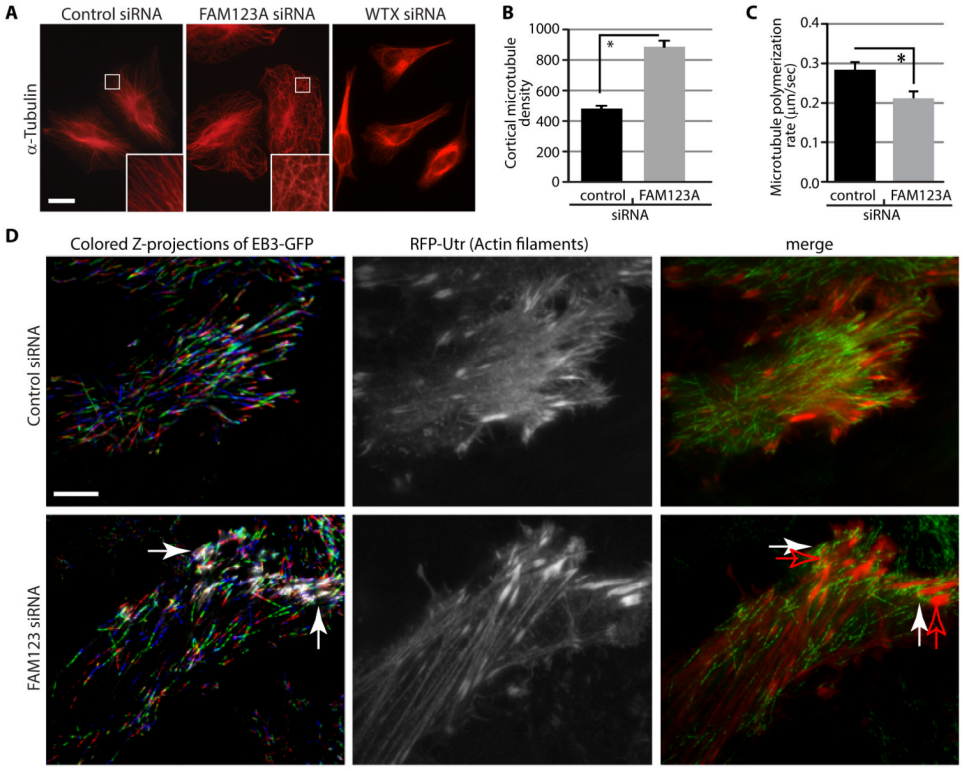

Figure 5. FAM123A depletion results in altered microtubule organization and increased actomysin contractility

(A) HeLa cells were transfected with the indicated siRNAs and stained with an anti-α-tubulin antibody. Images are representative of three independent biological replicates. **(B)** Plots of fluorescence intensity of α-tubulin staining in cells from panel (A). The integrated intensity was measured within a 5-μm^2 box at 5 μm distance from the cell periphery, in three different regions per cell for 23 control and FAM123A siRNA transfected cells.(*, $P<0.0001$; Welch-corrected *t* test) **(C)** Microtubule polymerization rates in siRNA transfected HeLa cells. 10 microtubules were measured in each cell. 9 cells were analyzed for each siRNA. (*, $P=0.0129$; Welch-corrected *t* test) **(D)** TIRF movies of siRNA-transfected HeLa cells expressing EB3-GFP (left) and RFP-Utr (middle). Left column; RGB-colorized 5 second Z-projections of EB3-GFP-labeled growing microtubule ends. Growing filaments are labeled either red, green or blue and overlapping stationary microtubule ends are white. Regions in cells lacking FAM123 where the microtubule ends are stationary (not assembling) are indicated (white arrows). Middle column; expressed RFP-Utr shows the filamentous actin near the cell substratum. Right column; a 15 frame (75 sec.) Z-stack of EB3-GFP (green) and RFP-Utr (red) over time. Stationary microtubule ends (white arrows) are in close apposition to actin bundles at the cell periphery (red open arrows).

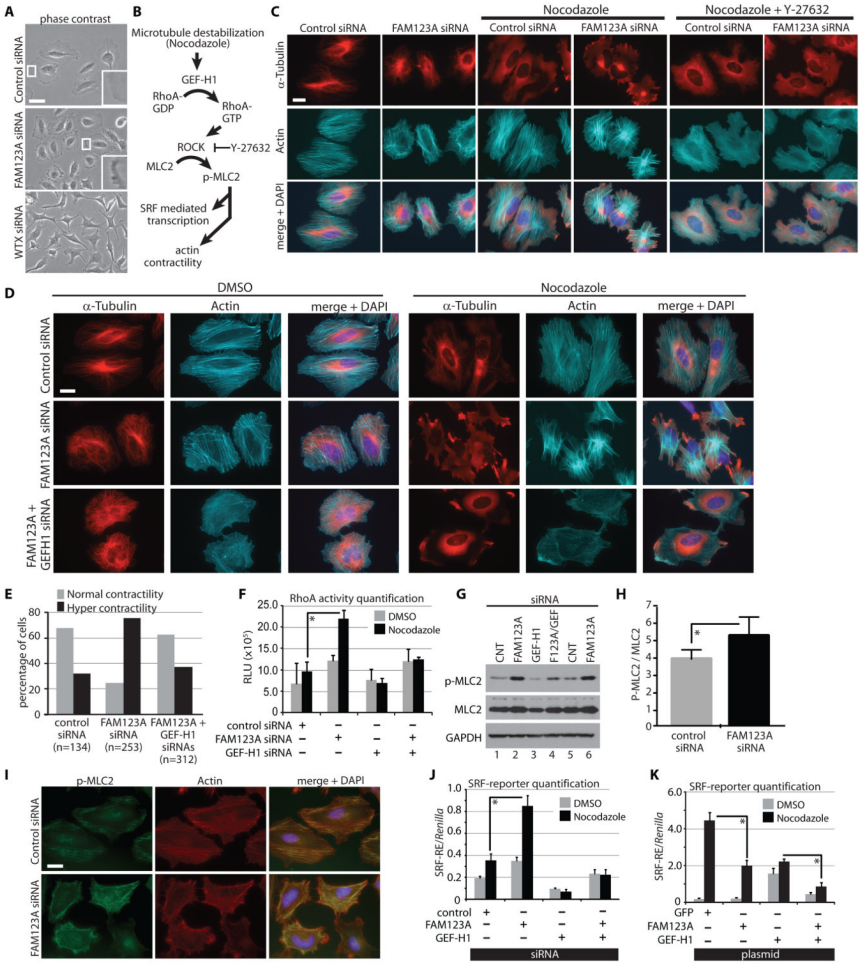

Figure 6. FAM123A regulates actomyosin contractility through GEF-H1

(A) HeLa cells transfected with siRNAs were imaged by phase-contrast microscopy. Images represent >3 biological replicates. Cell morphologies were confirmed with three different FAM123A siRNAs and 2 different WTX siRNAs. Scale bar 50μm. **(B)** The major signaling proteins connecting microtubule destabilization to actin contractility. **(C)** HeLa cells were transfected with control or FAM123A siRNA. Where indicated, cells were treated with the indicated drug before co-staining with an anti-α-tubulin antibody, AlexaFluor 647-conjugated phalloidin and DAPI. Images are representative of three independent biological replicate experiments. Scale bar 20μm. **(D)** siRNA-transfected HeLa cells were treated with nocodazole and co-stained with an anti-α-tubulin antibody, AlexaFluor 647-conjugated phalloidin and DAPI. Images are representative of 3 biological replicates. **(E)** Quantification of cell phenotypes in (D). Samples were scored in a blinded fashion by 3 independent investigators. n = number of cells scored. (**F**) siRNA-transfected HeLa cells were serum starved, treated with nocodazole, and analyzed for RhoA activity (P=0.002, Student's t-test of biological triplicate experiments) **(G)** siRNA-transfected HeLa cells were immunoblotted for the indicated proteins. Data are representative of 5 biological independent experiments. **(H)** Total MLC2 and phosphorylation of MLC2 at Ser^{19} from biological triplicate experiments were quantitated by LI-COR and plotted, (* P=0.0159; Student's t-test) **(I)** siRNA-transfected HeLa cells were stained with p-MLC Ser19 antibody, AlexaFluor 647-conjugated phalloidin and DAPI. Images are representative of 3 biological replicates **(J)** Quantitation of luciferase activity in HeLa cells expressing a SRF Firefly luciferase reporter

and a CMV-driven *Renilla* luciferase reporter. Cells were treated with DMSO or Nocodazole before luciferase quantitation. **(K)** Quantitation of luciferase activity in HeLa cells that were transiently transfected with the indicated expression construct(s), SRF firefly luciferase reporter and a CMV-driven *Renilla* luciferase reporter. (* $P<0.05$, Welch's corrected t-test of biological triplicates).

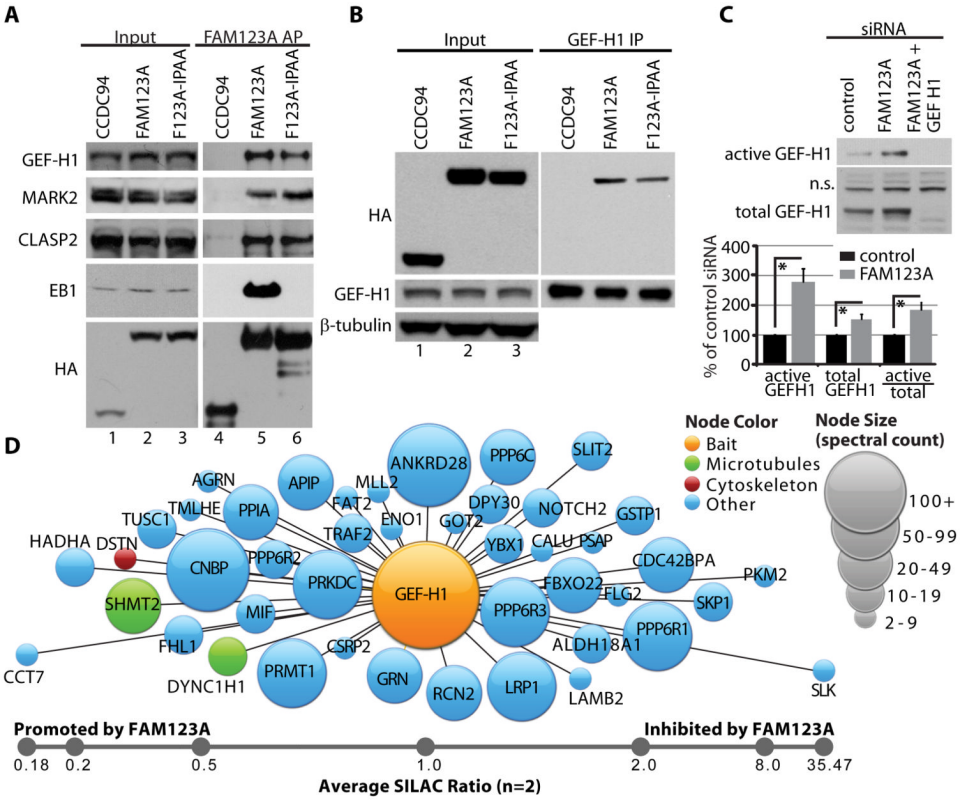

Figure 7. FAM123A binds to GEF-H1 and regulates its activity

(A) Streptavidin affinity pull-downs from HEK293T cells stably expressing SBPHA tagged CCDC94, FAM123A or FAM123A-IPAA were immunoblotted for endogenous associated proteins. **(B)** Using the HEK293T stable cell lines described in A, endogenous GEF-H1 was immunoprecipitated and protein complexes were analyzed by Western blot. **(C)** Active GEF-H1 was purified from siRNA-transfected HeLa cells by GST- $RhoA^{G17A}$ pulldown and immunoblotted. Active GEF-H1 and total cellular GEF-H1 was determined by densitometry (* $P<0.05$; Paired Student's t-test of 6 biological replicate experiments; error bars represent standard error). **(E)** The GEF-H1 protein interaction network, illustrating the FAM123A-sensitive interactions as determined by quantitative IP/MS. The average SILAC ratios from biological duplicate experiments are shown below the network.

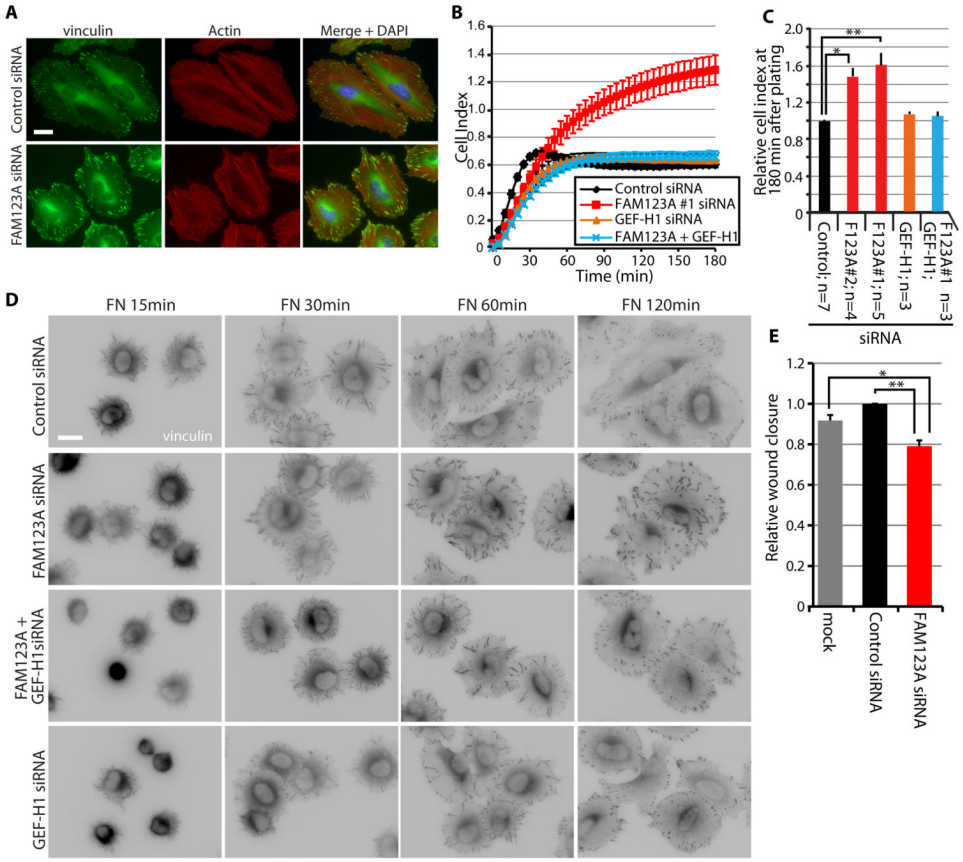

Figure 8. FAM123A regulates cell adhesion and migration

(A) siRNA-transfected HeLa cells were fixed and stained with an anti-vinculin antibody, Alexa Fluor 594-phalloidin and DAPI. Data represent 4 biological replicates. **(B)** Adhesion quantification of siRNA-transfected HeLa cells that were subjected to cell attachment with real-time acquisition of electrode impedance. **(C)** Histogram of relative impedance index 180 min after cell plating. Error bars reflect standard error across the biological replicates. (* P=0.005, * P=0.005; Paired Student's t-test; N = biological replicates) **(D)** siRNA-transfected HeLa cells were allowed to attach to fibronectin-coated coverslips for the indicated times before fixation and immunostaining with an anti-vinculin antibody. **(E).** HeLa cells transfected with control or FAM123A siRNA were scratch wounded and imaged over 24h. (* P=0.03 and ** P=0.018 by the Students t-test). N = 3 biological replicates.